nature nanotechnology

ARTICLES

https://doi.org/10.1038/s41565-017-0052-4

A broadband achromatic metalens in the visible

Shuming Wang[1,8], Pin Chieh Wu[2,8], Vin-Cent Su[3,8], Yi-Chieh Lai[4], Mu-Ku Chen[4], Hsin Yu Kuo[4], Bo Han Chen[4], Yu Han Chen[4], Tzu-Ting Huang[2], Jung-Hsi Wang[5], Ray-Ming Lin[6], Chieh-Hsiung Kuan[5], Tao Li[1,7], Zhenlin Wang[1,7], Shining Zhu[1,7] and Din Ping Tsai[2,4,6]*

Metalenses consist of an array of optical nanoantennas on a surface capable of manipulating the properties of an incoming light wavefront. Various flat optical components, such as polarizers, optical imaging encoders, tunable phase modulators and a retroreflector, have been demonstrated using a metalens design. An open issue, especially problematic for colour imaging and display applications, is the correction of chromatic aberration, an intrinsic effect originating from the specific resonance and limited working bandwidth of each nanoantenna. As a result, no metalens has demonstrated full-colour imaging in the visible wavelength. Here, we show a design and fabrication that consists of GaN-based integrated-resonant unit elements to achieve an achromatic metalens operating in the entire visible region in transmission mode. The focal length of our metalenses remains unchanged as the incident wavelength is varied from 400 to 660 nm, demonstrating complete elimination of chromatic aberration at about 49% bandwidth of the central working wavelength. The average efficiency of a metalens with a numerical aperture of 0.106 is about 40% over the whole visible spectrum. We also show some examples of full-colour imaging based on this design.

Metasurfaces are capable of tailoring light properties at subwavelength resolution[1,2], making them promising for developing flat optical components[3–5]. To date, a number of applications based on metasurfaces have been demonstrated through proper design of metasurface unit elements, such as polarization generators[6–8], optical imaging encoding[9–11], tunable optical components[12–15] and a retroreflector[16]. The great ability for super-resolution nanofabrication beyond the diffraction limit and surface plasmon focusing have also been shown based on plasmonic metasurfaces[17]. By producing a hyperbolical phase profile, metasurfaces can work as lenses (also referred to as metalenses) that are able to converge incident light beams with considerable efficiency[18,19]. Compared with conventional bulky lenses, which specifically rely on a polished surface profile on transparent optical materials to attain the required gradual phase change, metalenses are capable of focusing incident light with a more compact dimension. A metalens with extremely high numerical aperture (NA) has also been demonstrated[20], validating their great performance for future applications. However, the previously demonstrated metalenses still suffer from strong chromatic aberration. Some pioneering studies suggested optimizing arrangements of unit elements of the metalens to realize an achromatic metalens either at certain discrete wavelengths[21–24] or in a narrow bandwidth of the electromagnetic spectrum[25,26]. However, these metalenses with limited achromaticity are not competent enough for full-colour imaging applications. Very recently, we successfully demonstrated broadband achromatic metalenses by incorporating an integrated-resonant unit element (IRUE) with the Pancharatnam–Berry phase (PBP) method[27]. The required phase shift over the entire metalens surface was realized by carefully designing and arranging the IRUEs. As a proof-of-concept work, it was designed to operate in near-infrared region with a reflection scheme. Although the reflective metalens is useful in some cases, transmission optical components are much more attractive and highly desirable for practical applications, especially for metalenses working in the visible region[28,29].

In this study, we demonstrate a broadband achromatic metalens working in the visible light region in transmission mode. A lossless semiconductor material, gallium nitride (GaN), was used to construct unit elements to access waveguide-like resonant modes in the visible spectrum[18]. To introduce integrated resonances for required phase compensation, both solid and inverse structures[30] were implemented as the building blocks. Finally, we show full-colour imaging using achromatic and chromatic (which is designed via normal PBP-based metasurfaces[31,32]) metalenses to demonstrate that our design is promising for full-colour optical techniques and applications.

IRUEs with GaN nanopillars. In principle, a full-colour image without aberration effects can only be reconstructed through a perfect achromatic lens that is able to converge light at any wavelength within the working range into the same focal plane. The building blocks of our achromatic metalens are composed of solid (inset in Fig. 1a, also referred to as nanopillars) and inverse (inset in Fig. 1b) GaN nanostructures. To satisfy the phase requirement of achromatic metalenses, we employed a couple of resonant modes in the IRUEs. These IRUEs were carefully arranged and rotated on the metalens surface and consequently able to exactly provide the required phase compensation and basic phase corresponding to their spatial positions[27]. For the cases of plasmonic systems, the IRUEs were formed by a couple of specially placed nanorods, with near-field coupling among the nanostructures. Larger phase compensation can be directly realized by adding more resonators into the unit

[1]National Laboratory of Solid State Microstructures, College of Engineering and Applied Sciences, School of Physics, Nanjing University, Nanjing, China. [2]Research Center for Applied Sciences, Academia Sinica, Taipei, Taiwan. [3]Department of Electrical Engineering, National United University, Miaoli, Taiwan. [4]Department of Physics, National Taiwan University, Taipei, Taiwan. [5]Department of Electrical Engineering and Graduate Institute of Electronics Engineering, National Taiwan University, Taipei, Taiwan. [6]Department of Electronic Engineering, Chang Gung University, Taoyuan, Taiwan. [7]Collaborative Innovation Center of Advanced Microstructures, Nanjing, China. [8]These authors contributed equally: Shuming Wang, Pin Chieh Wu and Vin-Cent Su
*e-mail: dptsai@sinica.edu.tw

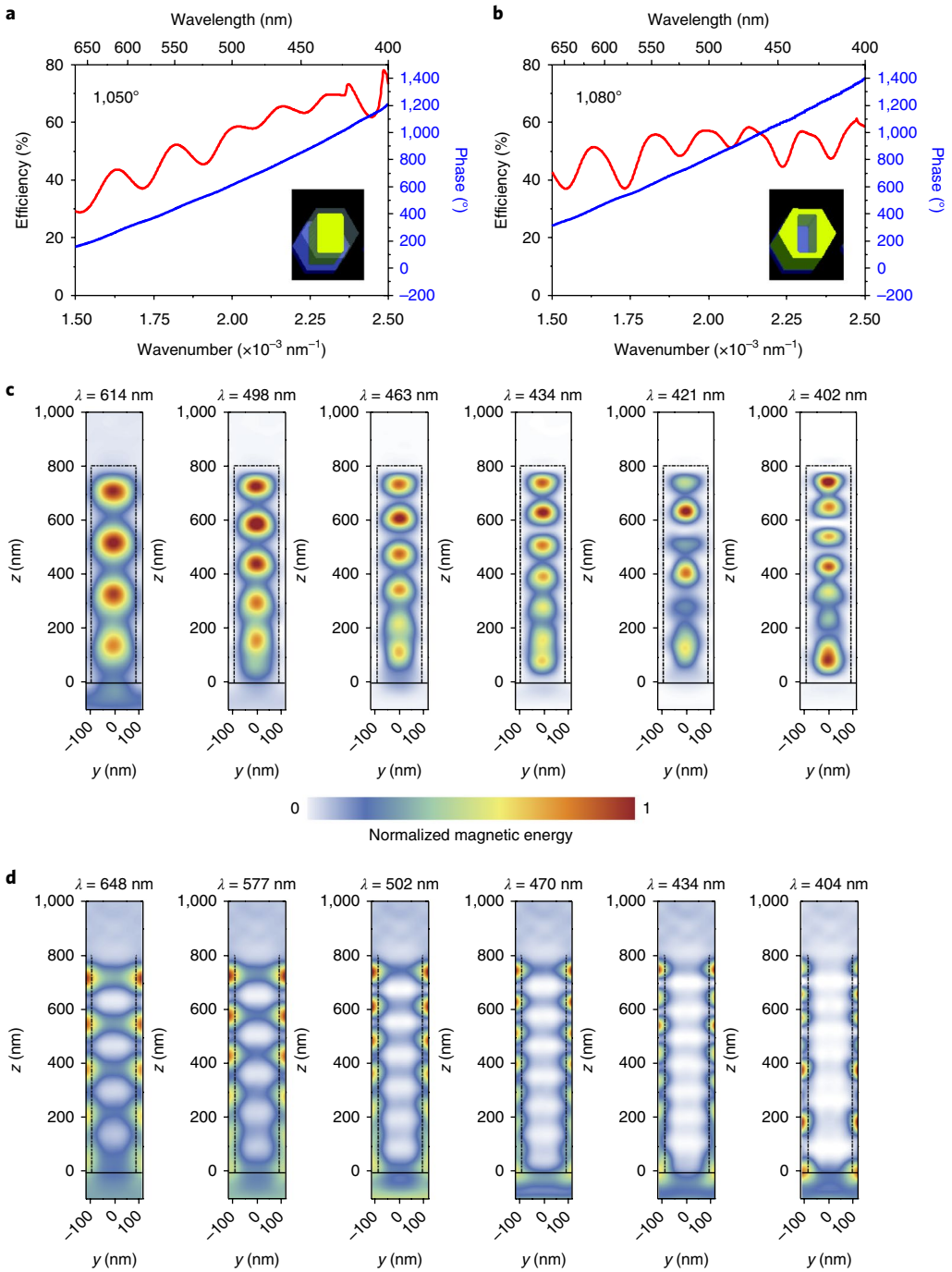

Fig. 1 | IRUEs for a broadband achromatic metalens in the visible light region. a,**b**, Circularly polarized conversion efficiency (red curves) and phase profile (blue curve) for IRUEs with phase compensation of 1,050° (**a**) and 1,080° (**b**). Insets illustrate the solid and inverse nanostructures, respectively. **c**,**d**, Normalized magnetic energy for phase compensation of 1,050° (**c**) and 1,080° (**d**) at different incident wavelengths. The black dashed line indicates the boundary of GaN structures. The thickness of all GaN nanopillars is fixed at 800 nm, standing on an Al_2O_3 substrate.

cells. In contrast, optical coupling among dielectric nanopillars is weak because of their high refractive index compared with the surrounding environment[33,34]. Moreover, the waveguide-like cavity resonances in nanopillars show that the induced optical fields are highly concentrated inside the dielectric structures, resulting in the negligible interaction with their neighbours[34]. Instead of introducing more resonators, one can also acquire large phase compensation with GaN nanopillars by exciting higher orders of waveguide-like cavity resonances, which can be realized by directly increasing the height of the nanopillars. Figure 1c,d shows the right-hand circular polarization to left-hand circular polarization conversion efficiency (red curves) and phase profile (blue curves) for phase compensation of 1,050° (Fig. 1c) and 1,080° (Fig. 1d). More details of all GaN IRUEs can be found in Supplementary Section 1. The ripples result from the excitation of multi-resonances inside the GaN nanopillars, which can be verified by checking the near-field distribution, as shown in Fig. 1c,d. The chosen wavelengths correspond to the efficiency peaks and dips, indicating that waveguide-like cavity resonances are supported in either the GaN nanopillar (solid cases) or the surrounding GaN (inverse cases).

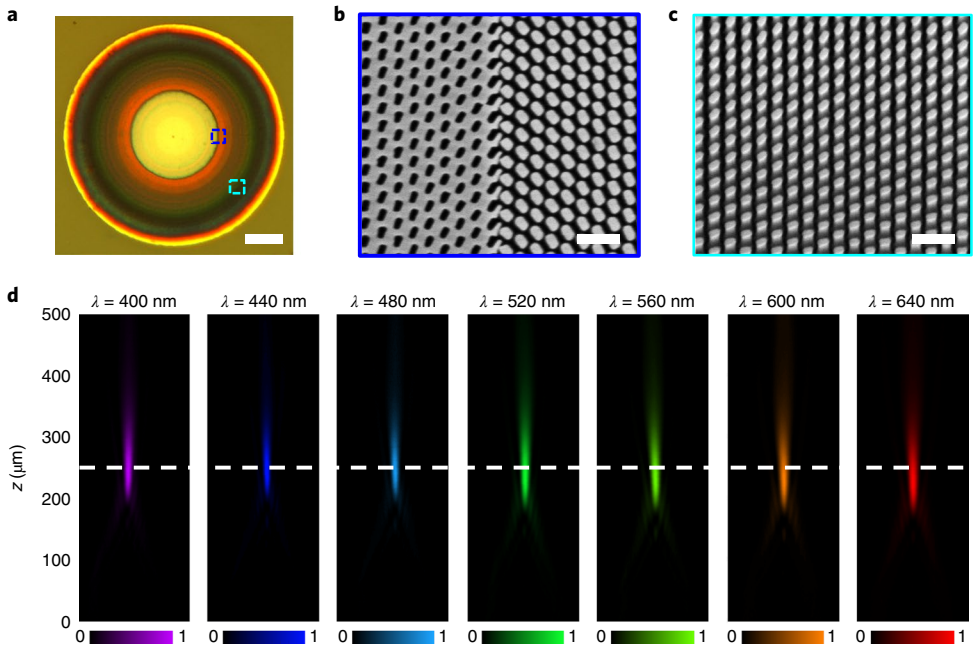

Fig. 2 | Experimental verification of achromatic metalenses. a, Optical image of the fabricated achromatic metalens with NA = 0.106. The dashed squares indicate the position of the SEM images shown in **b** and **c**. Scale bar: 10 μm. **b**,**c**, Zoomed-in SEM images at the boundary of nanopillars and Babinet structures (top view, **b**) and the region of nanopillars (tilted view, **c**). Scale bars: 500 nm. **d**, Experimental light intensity profiles for the achromatic metalens with NA = 0.106 at various incident wavelengths. The white dashed line indicates the position of the focal plane.

Characteristics of broadband achromatic metalens. The design principles of a broadband achromatic metalens have been previously reported[27]. In brief, we started with the phase profile of a general metalens and incorporated an additional phase shift. The phase profile of the achromatic metalens, φ_{AL} can be described by equation (1)[22,27,35,36]:

$$\varphi_{AL}(r,\lambda) = -\left[\frac{2\pi}{\lambda}\left(\sqrt{r^2+f^2}-f\right)\right] + \varphi_{shift}(\lambda) \quad (1)$$

where $r=\sqrt{x^2+y^2}$ is the distance between an arbitrary point and the centre of the achromatic metalens surface (assuming the surface of the metalens is located in the $z=0$ plane). λ and f are the working wavelength in free space and the designed focal length, respectively. The additional phase shift exhibits an inversely linear relationship with the wavelength λ, that is $\varphi_{shift}(\lambda)=\frac{a}{\lambda}+b$, with $a=\delta\frac{\lambda_{min}\lambda_{max}}{\lambda_{max}-\lambda_{min}}$ and $b=-\delta\frac{\lambda_{min}}{\lambda_{max}-\lambda_{min}}$. The δ denotes the largest additional phase shift while λ_{min} and λ_{max} are the boundaries of the wavelength band of interest. To satisfy the phase requirement as described in equation (1), we divided it into two parts:

$$\varphi_{AL}(r,\lambda) = \varphi_{L}(r,\lambda_{max}) + \Delta\varphi'(r,\lambda) \quad (2)$$

where

$$\varphi_{L}(r,\lambda_{max}) = -\left[\frac{2\pi}{\lambda_{max}}\left(\sqrt{r^2+f^2}-f\right)\right]$$

and $\Delta\varphi'(r,\lambda) = -[2\pi(\sqrt{r^2+f^2}-f)]\left(\frac{1}{\lambda}-\frac{1}{\lambda_{max}}\right)+\varphi_{shift}(\lambda)$. The first term in equation (2) is dispersionless and the second term is wavelength dependent[29]. The first term is obtained using the PBP method, while the second term can be realized through IRUEs. The phase difference between the maximum and the minimum wavelengths within the working bandwidth (defined as phase compensation, which is also a function of spatial position on the metalens surface) is consequently compensated by the integrated resonances.

Figure 2a shows an optical microscopic image of an achromatic metalens sample with a NA of 0.106. Owing to the introduction of φ_{shift}, the inverse GaN structure (which is able to offer larger phase compensation, see Supplementary Section 1) plays the dominant role in the central part of the achromatic metalens. Details about the fabrication parameters can be found in Supplementary Fig. 3. Figure 2b,c shows the scanning electron microscope (SEM) images of the fabricated sample. From such images, we observe that both the solid and inverse GaN-based IRUEs are well defined, showing the precise fabrication technique with several hard mask transfer and etching processes. It is worth mentioning that our approach, compared with the specific top-down lithography approach using atomic layer deposition for visible metalenses[37], has significant advantages of low-cost and semiconductor foundry compatibility, which definitely would benefit the development of flat optical systems in real life.

The light intensity profile after the incident beam had passed through the achromatic metalens was experimentally examined using the optical system shown in Supplementary Fig. 4. To properly select the circular polarization state at different focal planes, a couple of lenses, a quarter-wave plate and a linear polarizer were mounted on a motorized stage and moved together along the light propagation direction. Figure 2d shows the measured cross-sectional intensity profiles for the achromatic metalens with a designed focal length $f=235$ μm and NA = 0.106. For the wavelength region ranging from 400 to 660 nm, the brightest spots were all close to the designed position (white dashed line). To further verify the optical performance of achromatic metalenses fabricated from GaN-based structures using the design principle of IRUEs, three lenses with different NA values were fabricated and experimentally examined (see Supplementary Fig. 5 for sample images). We found that the focal lengths remained unchanged within the entire range of the visible spectrum for all of the designed achromatic metalenses, as shown in Supplementary Fig. 6. This can be more clearly evaluated by examining focal length as a function of incident wavelength.

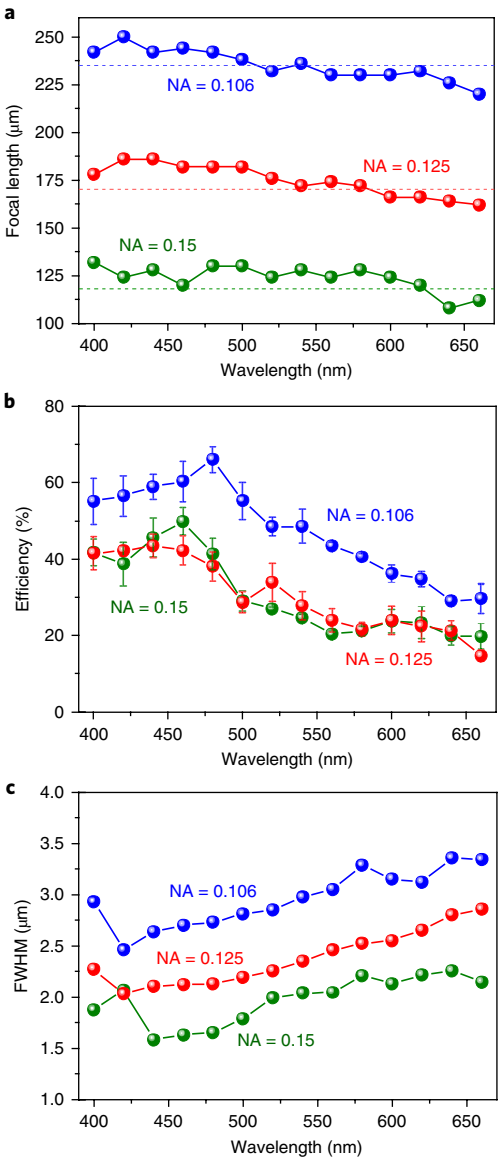

Fig. 3 | Performance of broadband achromatic metalens. a–c, Measured focal length (**a**), operation efficiency (**b**) and FWHM (**c**) as a function of incident wavelength obtained from three achromatic metalenses with different NA values. Error bars are the standard deviation of measured efficiencies from four different samples.

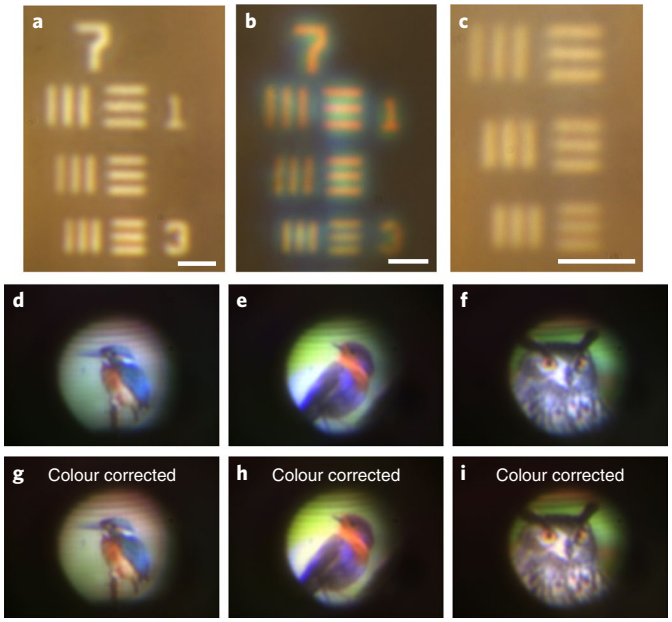

Fig. 4 | Imaging using a visible achromatic metalens with NA = 0.106. **a–c**, Image of 1951 USAF resolution test chart taken from achromatic (**a**,**c**) and chromatic (**b**) metalenses. Scale bars: 4 μm. **d–i**, Full-colour Alcedinidae (**d**,**g**), *Erithacus rubecula* (**e**,**h**) and Eurasian eagle owl (**f**,**i**) images formed by the achromatic metalens. Captured images from achromatic metalens before (**d–f**) and after (**g–i**) colour correction.

Figure 3a shows the focal length as a function of incident wavelength for three achromatic metalenses. As predicted, all focal lengths remained almost unchanged when the incident wavelength was varied over the entire range of the visible spectrum. The working bandwidth was about 49% of the central wavelength (530 nm). Figure 3b shows the measured focusing efficiency for the three achromatic metalenses. The efficiency is defined as the ratio of the optical power of the focused circularly polarized beam to the optical power of the incident beam with opposite helicity[20]. The highest efficiency can be up to 67%, while the average efficiency is about 40% over the whole working bandwidth. The efficiency spectra vary with working wavelength, which can arise from two issues: fluctuations in the polarization conversion efficiency spectra of IRUEs (see Supplementary Fig. 2) and imperfections in the fabricated samples. The first issue can be addressed by further optimizing the structural configuration to make the efficiency spectra smoother. Regarding the second issue, to fairly evaluate the working efficiency of achromatic metalenses with imperfect fabrication, each point shown in Fig. 3b is the average efficiency measured from four different samples. It can also be seen that the working efficiency is relatively low in red light, regardless of the NA of the metalens. This is mainly due to the strong radiative recombination and non-unity quantum yield of the GaN thin film[38]. To improve the working efficiency in red light, the quality of the GaN thin film can be improved by optimizing the epitaxial growth process[18]. All the measured focal spots show nearly ideal full-width half-maximum (FWHM) values close to the diffraction-limited values $\left(\frac{\lambda}{2\mathrm{NA}}\right)$, as shown in Fig. 3c. It is worth mentioning that the size of the achromatic metalenses is limited by the largest phase compensation, which can be significantly extended by introducing more integrated resonances into the unit elements. For example, one can either reliably increase the thickness of GaN structures or use asymmetric shapes as the unit elements to excite more plentiful resonant modes inside the dielectric structures.

Imaging with visible achromatic metalenses. To demonstrate the practical use of optical imaging, we fabricated a chromatic metalens (designed with normal PBP metasurfaces) and compared its imaging performance with the achromatic metalens. The chromatic metalens (sample images can be found in Supplementary Fig. 7) is designed for green light ($\lambda = 500$ nm, central wavelength of visible spectrum) with the same diameter and focal length as our achromatic sample.

First, the 1951 United State Air Force (USAF) resolution test chart was used as the imaging target, and was illuminated by a halogen light source. The optical configuration is shown in Supplementary Fig. 8. Owing to the use of the PBP method, the images formed by the achromatic metalens can only be projected with circularly polarized light. A quarter-wave plate consequently was used to filter the image and improve the imaging quality. Figure 4a,b shows the results from the achromatic and chromatic metalenses. Owing to the strong chromatic effect, the edges of the lines in the images taken with the chromatic metalens show diverse colours, leading

to vague features in images. In contrast, the image taken with the achromatic metalens exhibits extremely clear line features, showing the chromatic effect is completely eliminated. We subsequently took another image with smaller line features using the achromatic metalens, as shown in Fig. 4c. The smallest features of objects that could be resolved were lines with widths of ~2.19 μm, which is consistent with the measured FWHM shown in Fig. 3c. For an achromatic metalens working in transmission mode, a clear colourful image can be obtained on the imaging plane. For example, Fig. 4d–f shows the full-colour images formed through our achromatic metalens. Compared with the original pictures (which can be found in Supplementary Fig. 9), the slight difference in colour is mainly from the efficiency variation of the fabricated achromatic metalens (see Fig. 3b). This can be corrected by compensating the intensity at three preliminary colours. After colour correction, the images show more reliable colours compared with the original pictures, as shown in Fig. 4g–i. The intensity ratio of blue (440 nm) and red (660 nm) and green (540 nm) and red was modulated by 0.75 and 0.83, respectively, which is quite consistent with the measured efficiencies shown in Fig. 3. All the images shown in Fig. 4 demonstrate the effectiveness of eliminating the chromatic effect by incorporating IRUEs with a PBP method over the entire visible spectrum.

Conclusions

In summary, we have shown a broadband achromatic metalens working in the visible light region by utilizing a series of GaN-based resonant elements. The required phase profile for realizing an achromatic metalens is achieved by incorporating integrated resonances with a PBP method. Using the 1951 USAF resolution test chart, we have demonstrated full-colour imaging performance in transmission mode. Considering its compact size, this achromatic metalens can be used in metalens arrays, which may be promising for achromatic imaging in a light field camera[39]. Moreover, the performance and size of our achromatic metalens can be improved by combining it with conventional optical devices. Finally, the low-cost and semiconductor manufacture compatibility makes our metalens suitable for applications in nanophotonics and integrated optics in the visible.

Data availability. The data that support the findings of this study are available from the corresponding author on reasonable request.

Received: 5 November 2017; Accepted: 15 December 2017;
Published online: 29 January 2018

References

1. Luo, X. G. Principles of electromagnetic waves in metasurfaces. Sci. China Phys. *Mech. Astron.* **58**, 594201 (2015).
2. Pu, M. et al. Catenary optics for achromatic generation of perfect optical angular momentum. *Sci. Adv.* **1**, e1500396 (2015).
3. Hsiao, H.-H., Chu, C. H. & Tsai, D. P. Fundamentals and applications of metasurfaces. *Small Methods* **1**, 1600064 (2017).
4. Genevet, P., Capasso, F., Aieta, F., Khorasaninejad, M. & Devlin, R. Recent advances in planar optics: from plasmonic to dielectric metasurfaces. *Optica* **4**, 139–152 (2017).
5. Yu, N. & Capasso, F. Flat optics with designer metasurfaces. *Nat. Mater.* **13**, 139–150 (2014).
6. Wu, P. C. et al. Versatile polarization generation with an aluminum plasmonic metasurface. *Nano Lett.* **17**, 445–452 (2017).
7. Li, L. et al. Plasmonic polarization generator in well-routed beaming. *Light. Sci. Appl.* **4**, e330 (2015).
8. Wu, P. C. et al. Broadband wide-angle multifunctional polarization converter via liquid-metal-based metasurface. *Adv. Opt. Mater.* **5**, 1600938 (2017).
9. Li, X. et al. Multicolor 3D meta-holography by broadband plasmonic modulation. *Sci. Adv.* **2**, e1601102 (2016).
10. Huang, L. et al. Broadband hybrid holographic multiplexing with geometric metasurfaces. *Adv. Mater.* **27**, 6444–6449 (2015).
11. Huang, Y.-W. et al. Aluminum plasmonic multicolor meta-hologram. *Nano Lett.* **15**, 3122–3127 (2015).
12. Wu, P. C., Papasimakis, N. & Tsai, D. P. Self-affine graphene metasurfaces for tunable broadband absorption. *Phy. Rev. Appl.* **6**, 044019 (2016).
13. Sherrott, M. C. et al. Experimental demonstration of >230° phase modulation in gate-tunable graphene–gold reconfigurable mid-infrared metasurfaces. *Nano Lett.* **17**, 3027–3034 (2017).
14. Thyagarajan, K., Sokhoyan, R., Zornberg, L. & Atwater, H. A. Metasurfaces: millivolt modulation of plasmonic metasurface optical response via ionic conductance. *Adv. Mater.* **29**, 1701044 (2017).
15. Huang, Y.-W. et al. Gate-tunable conducting oxide metasurfaces. *Nano Lett.* **16**, 5319–5325 (2016).
16. Arbabi, A., Arbabi, E., Horie, Y., Kamali, S. M. & Faraon, A. Planar metasurface retroreflector. *Nat. Photon.* **11**, 415–420 (2017).
17. Luo, X. & Ishihara, T. Surface plasmon resonant interference nanolithography technique. *Appl. Phys. Lett.* **84**, 4780–4782 (2004).
18. Chen, B. H. et al. GaN metalens for pixel-level full-color routing at visible light. *Nano Lett.* **17**, 6345–6352 (2017).
19. Arbabi, A., Horie, Y., Bagheri, M. & Faraon, A. Dielectric metasurfaces for complete control of phase and polarization with subwavelength spatial resolution and high transmission. *Nat. Nanotech.* **10**, 937–943 (2015).
20. Khorasaninejad, M. et al. Metalenses at visible wavelengths: diffraction-limited focusing and subwavelength resolution imaging. *Science* **352**, 1190–1194 (2016).
21. Khorasaninejad, M. et al. Achromatic metasurface lens at telecommunication wavelengths. *Nano Lett.* **15**, 5358–5362 (2015).
22. Aieta, F., Kats, M. A., Genevet, P. & Capasso, F. Multiwavelength achromatic metasurfaces by dispersive phase compensation. *Science* **347**, 1342–1345 (2015).
23. Avayu, O., Almeida, E., Prior, Y. & Ellenbogen, T. Composite functional metasurfaces for multispectral achromatic optics. *Nat. Commun.* **8**, 14992 (2017).
24. Hu, J., Liu, C.-H., Ren, X., Lauhon, L. J. & Odom, T. W. Plasmonic lattice lenses for multiwavelength achromatic focusing. *ACS Nano* **10**, 10275–10282 (2016).
25. Khorasaninejad, M. et al. Achromatic metalens over 60 nm bandwidth in the visible and metalens with reverse chromatic dispersion. *Nano Lett.* **17**, 1819–1824 (2017).
26. Arbabi, E., Arbabi, A., Kamali, S. M., Horie, Y. & Faraon, A. Controlling the sign of chromatic dispersion in diffractive optics with dielectric metasurfaces. *Optica* **4**, 625–632 (2017).
27. Wang, S. et al. Broadband achromatic optical metasurface devices. *Nat. Commun.* **8**, 187 (2017).
28. Khorasaninejad, M. et al. Multispectral chiral imaging with a metalens. *Nano Lett.* **16**, 4595–4600 (2016).
29. Khorasaninejad, M., Ambrosio, A., Kanhaiya, P. & Capasso, F. Broadband and chiral binary dielectric meta-holograms. *Sci. Adv.* **2**, e1501258 (2016).
30. Hentschel, M., Weiss, T., Bagheri, S. & Giessen, H. Babinet to the half: coupling of solid and inverse plasmonic structures. *Nano Lett.* **13**, 4428–4433 (2013).
31. Wen, D. et al. Metasurface device with helicity-dependent functionality. *Adv. Opt. Mater.* **4**, 321–327 (2016).
32. Zheng, G. et al. Metasurface holograms reaching 80% efficiency. *Nat. Nanotech.* **10**, 308–312 (2015).
33. Kamali, S. M., Arbabi, A., Arbabi, E., Horie, Y. & Faraon, A. Decoupling optical function and geometrical form using conformal flexible dielectric metasurfaces. *Nat. Commun.* **7**, 11618 (2016).
34. Arbabi, A., Horie, Y., Ball, A. J., Bagheri, M. & Faraon, A. Subwavelength-thick lenses with high numerical apertures and large efficiency based on high-contrast transmitarrays. *Nat. Commun.* **6**, 7069 (2015).
35. Wang, P., Mohammad, N. & Menon, R. Chromatic-aberration-corrected diffractive lenses for ultra-broadband focusing. *Sci. Rep.* **6**, 21545 (2016).
36. Li, Y. et al. Achromatic flat optical components via compensation between structure and material dispersions. *Sci. Rep.* **6**, 19885 (2016).
37. Devlin, R. C., Khorasaninejad, M., Chen, W. T., Oh, J. & Capasso, F. Broadband high-efficiency dielectric metasurfaces for the visible spectrum. *Proc. Natl. Acad. Sci. USA* **113**, 10473–10478 (2016).
38. Goldys, E. M. et al. Analysis of the red optical emission in cubic GaN grown by molecular-beam epitaxy. *Phys. Rev. B* **60**, 5464–5469 (1999).
39. Ng, R. et al. *Light Field Photography with a Hand-Held Plenoptic Camera* Stanford University Computer Science Tech Report CSTR 2005-02 (Stanford Univ., 2005).

Acknowledgements

The authors acknowledge financial support from The National Key R&D Program of China (2017YFA0303700, 2016YFA0202103), National Natural Science Foundation of China (no. 11674167, 11621091, 11774164, 11322439), Ministry of Science and Technology, Taiwan (grant no. MOST-106-2745-M-002-003-ASP) and Academia Sinica (grant no. AS-103-TP-A06). T.L. thanks the support from Dengfeng Project B of Nanjing University. The authors are also grateful to the National Center for Theoretical Sciences, NEMS Research Center of National Taiwan University, National Center for High-Performance Computing, Taiwan, and Research Center for Applied Sciences, Academia Sinica, Taiwan for their support.

Author contributions

S.W. and P.C.W. developed the theoretical aspects, performed the numerical design, optical measurement and data analysis, and wrote the manuscript. V.-C.S. performed the sample preparation. Y.-C.L., M.-K.C. and H.Y.K. built up the optical system for measurement. B.H.C., Y.H.C. and T.-T.H. performed the numerical simulation and data analysis. J.-H.W., R.-M.L. and C.-H.K. provided GaN film and performed the sample preparation. T.L., Z.W. and S.Z. organized the project, designed experiments, analysed the results and prepared the manuscripts. D.P.T. organized the project, designed and developed the theoretical model, numerical design and optical measurement, analysed the results and prepared the manuscript. All authors discussed the results and commented on the manuscript.

Competing interests

The authors declare no competing financial interests.

Additional information

Supplementary information is available for this paper at https://doi.org/10.1038/s41565-017-0052-4.

Reprints and permissions information is available at www.nature.com/reprints.

Correspondence and requests for materials should be addressed to D.P.T.

Publisher's note: Springer Nature remains neutral with regard to jurisdictional claims in published maps and institutional affiliations.